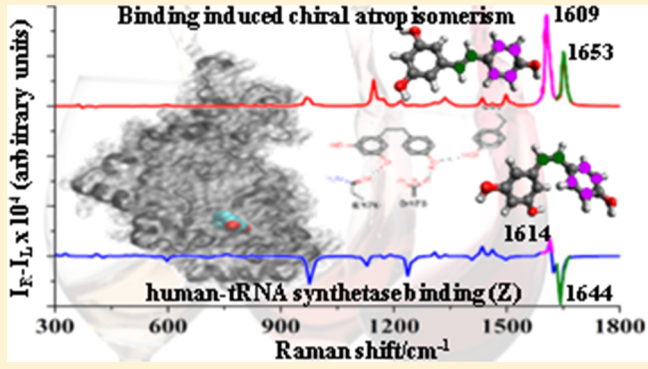


Resveratrol's Hidden Hand: A Route to the Optical Detection of Biomolecular Binding

Subhojyoti Chatterjee,[†] Seth Olsen,^{†,‡,§,#} Ewan W. Blanch,[§] and Feng Wang^{*,†,||,⊥,#}[†]Molecular Model Discovery Laboratory, Department of Chemistry and Biotechnology, Faculty of Science, Engineering and Technology, Swinburne University of Technology, Hawthorn, P.O. Box 218, Melbourne, VIC 3122, Australia[‡]School of Mathematics and Physics, The University of Queensland, Brisbane, QLD 4072, Australia[§]School of Science, RMIT University, Melbourne, VIC 3001, Australia^{||}School of Chemistry and [⊥]School of Physics, University of Melbourne, Parkville, VIC 3052, Australia

Supporting Information

ABSTRACT: Resveratrol is a stilbenoid phytoalexin with promising myriad health benefits predominantly contributed by the *trans* (*E*) diastereomeric form. A recent study has implicated the *cis* (*Z*) diastereomer in human health. This stereoisomer binds with high affinity to human tyrosyl-tRNA synthetase, initiating a downstream cascade that promotes the expression of genes associated with the cellular stress response. We discovered that the nonplanar structure of the *cis*-resveratrol conformer possesses certain chiral signals in its simulated vibrational circular dichroism (VCD) and Raman optical activity (ROA) spectra. These features may be used for the optical detection of the binding event and in understanding the more diversified biological roles of *trans*-resveratrol over *cis*-resveratrol. We use a density functional theory model, which is validated against the known results for the *E* diastereomer. The *Z* diastereomer is significantly nonplanar and can exist in two helical atropisomeric forms. These forms exchange rapidly in solution, but only one is observed to bind with the synthetase. This suggests that the binding may generate an enantiomeric excess, leading to detectable changes in the vibrational optical activity spectra. We identify candidate features at 998, 1649, and 1677 cm⁻¹ in the ROA and at 1642 and 3834 cm⁻¹ in the VCD spectra of *Z*-resveratrol that may be useful for this purpose.



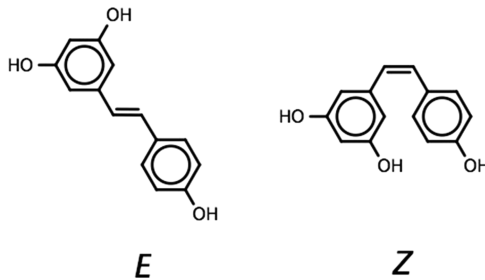
1. INTRODUCTION

Resveratrol (RSVL, 3,5,4'-trihydroxystilbene, see Scheme 1) is a stilbenoid phytoalexin produced in many food plants as a response to a physical insult and/or a pathogenic infection.^{1,2} It emerged into popular consciousness after 1993, when it was found that it inhibited the oxidation of low-density lipoproteins (a step in the development of arteriosclerosis and coronary heart disease).³ As an important constituent of red wine, it was

proposed to resolve the “French paradox” (referring to the low occurrence of coronary atherosclerosis in the French populace despite an elevated exposure to risk factors in the diet).⁴ Over the last two decades, it has re-emerged multiple times in connection with studies indicating possible health benefits.^{5–18}

As indicated in Scheme 1, resveratrol (RSVL) can exist in one of the two diastereomeric forms: *E* and *Z*. Reports of biological activity have concentrated overwhelmingly on *E*, which is the more stable form.^{19–21} The *Z* diastereomer occurs in significant amounts in red wines but only slightly in grape berry extracts.²² The *E* and *Z* diastereomers interchange through a photoisomerization reaction in permissive media.^{23,24} We previously studied the structures and NMR spectroscopies of *E*- and *Z*-resveratrol, indicating that the geometric isomers indeed possess some important different properties rather than merely the orientations of the hexagon rings.²¹ In a molecular dynamics simulation for the resveratrol isomer recognition by

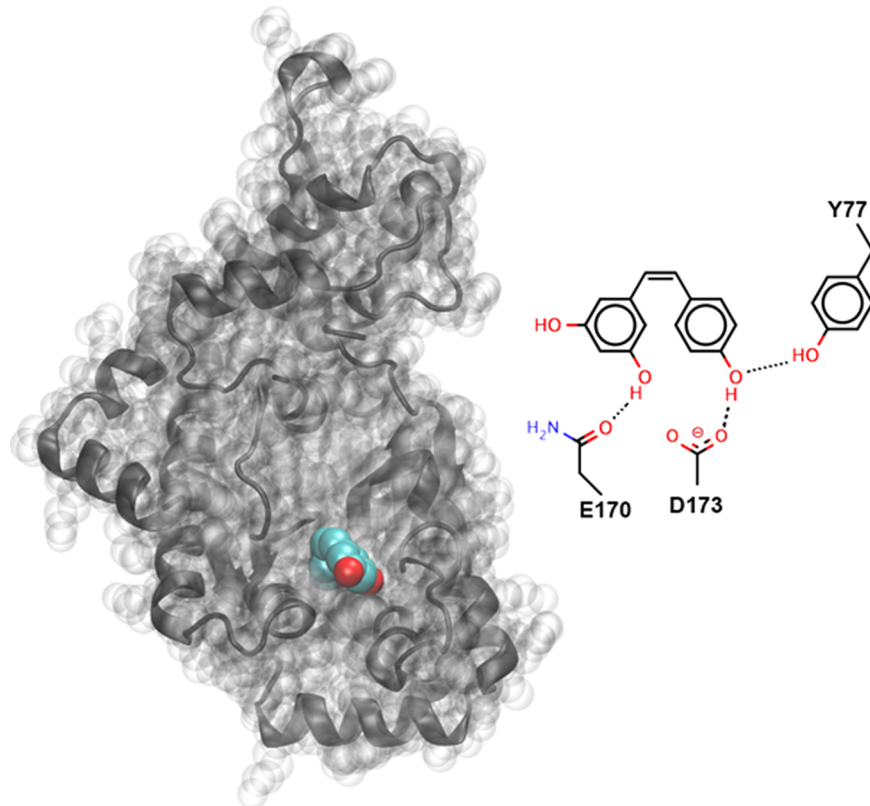
Scheme 1. Chemical Structures of the *E* and *Z* Diastereomers of Resveratrol (RSVL)



Received: October 17, 2017

Revised: February 15, 2018

Published: February 17, 2018

Scheme 2. Illustration of P-Z-Resveratrol Bound to the Human Tyrosyl-tRNA Synthetase (Protein Data Bank, PDB: 4Q93)^a

^aInset shows key ligation interactions with surrounding residues in the pocket.

the human estrogen receptor- α (ER- α), it distinguishes *E*-resveratrol and two forms of the *Z*-resveratrol stereoisomers forming different number of hydrogen bonds when being docked at the ER- α active sites.²⁵

Despite many documented studies suggesting possible health benefits of resveratrol, the mechanism by which such benefits are induced is still unclear. In particular, it is still not clear what the primary binding target for resveratrol is and how the binding event triggers any downstream benefits.⁷ Early suggestions were that resveratrol activates proteins responsible for the regulation of mitochondrial energy metabolism.^{8,11,26–28} Later, attention turned away from the mitochondrial metabolism and focused instead on the possibility that resveratrol may promote a family of genes associated with cellular stress response.^{28,29}

It has recently been shown that *Z*-resveratrol binds strongly to, and inhibits, the human tyrosyl-tRNA synthetase,³⁰ as indicated in Scheme 2. Resveratrol binding redirects the tRNA synthetase to a nuclear function, an event known to occur under stressful conditions.³¹ A co-crystal structure of the resveratrol-bound synthetase indicated a binding-dependent conformational change that opens up a pocket capable of accommodating *Z*-but not *E*-resveratrol. It was suggested that this may drive the formation and accumulation of the *Z* diastereomer from *E*.

If binding to the tRNA synthetase drives the formation of *Z*, then the growth of spectral features unique to *Z* may provide a means to detect the binding using optical techniques. In this article, we focus on the simulation of vibrational spectra of the *Z* diastereomer, with the intention of identifying if and which spectral signals may be used to detect its accumulation in the

bound state. We employ a density functional theory (DFT) model, which we assessed using the published spectra of the *E* isomer.^{21,32} We then identify features in the IR and Raman scattering spectra, which distinguish the *E* and *Z* isomers. The *Z* isomer has an exaggerated nonplanarity in the ground-state, relative to *E*, that arises from steric hindrance between the rings connected by the stilbene bond.²¹ The nonplanarity causes either diastereomer to exist in one of the two possible helical atropisomers, *P* and *M*. The atropisomerization was not observable in solution because of the fast exchange, but only one atropisomer was observed in co-crystal structures with the human-tRNA synthetase.³⁰ We show that the helical nonplanarity of *Z* gives rise to distinct features in the vibrational optical activity (VOA) spectra of this species and suggest that the observation of optical activity in these regions may be useful for detecting the accumulation of bound *Z*-resveratrol.

2. METHODS

We have simulated vibrational spectra of *Z*- and *E*-resveratrol using a density functional theory (DFT) model based on the hybrid Becke three-parameter Lee–Yang–Parr (B3LYP)^{33,34} functional combined with the 6-311++G** basis set,^{35–37} which is larger in comparison to the previously studied 6-31G* basis set.³⁸ The B3LYP model offers an accurate and effective choice for the prediction of molecular vibrational properties, as indicated by different studies on vibrational spectroscopy.^{32,38–43} We optimized structures of *Z*- and *E*-resveratrol on the ground-state energy surface. The structures were reported in our recent study.²¹ All quantum mechanical calculations were carried out using Gaussian09 computational chemistry software.⁴⁴

The IR/vibrational circular dichroism (VCD) and Raman/Raman optical activity (ROA) (at 532 nm excitation wavelength) spectral simulations were performed in both vacuum and solvent phases (i.e., acetonitrile, $\epsilon = 37.5$). The VCD was calculated according to Stephen's magnetic field perturbation theory^{45,46} using the gauge-including atomic orbital method as implemented within the DFT framework in Gaussian. Specifically, Raman intensities were calculated from the calculation of the force constants, whereas ROA intensities were calculated from the calculations of normal modes. The latter (ROA) calculation new polarizability derivatives (and the other two tensor derivatives for ROA) were computed and combined with the force constants in predicting intensities and spectra, which are included in the standard Gaussian programs. Vibrational frequencies provided by the B3LYP/6-311++G** model were scaled by a factor of 0.98. All spectra were generated from the calculated intensities by convolution using a Lorentzian line shape function with 4 cm^{-1} full width at half-maximum (FWHM). The FWHM in the present study is 4 cm^{-1} rather than the default 10 cm^{-1} , as it produces more appropriate spectra for the experiment.

Figure S1 provides a test of the vibrational spectra model by comparing calculated vibrational (IR and Raman) spectra for the *E* diastereomer with the spectra published in the literature.³² The simulated spectra shown are from the calculations in vacuum. We also compared these spectra against the spectra simulated in acetonitrile solution (Table S1) using the conductor-like polarizable continuum model⁴⁷ and found that these spectra qualitatively agree. In Figure S1, most spectral peaks in the experimental spectra are identifiable with peaks in the simulated spectra. This benchmark suggests that our use of the B3LYP/6-311++G** model is a robust tool for simulating the vibrational spectra and temperature does not significantly affect the spectra. This DFT-based model is attractive in terms of accuracy and computational effort, as discussed above and also pointed out by Gawronski et al.⁴⁸ We confirmed this in preliminary IR spectra recorded on samples of *E*- and *Z*-resveratrol isolated by high-performance liquid chromatography (HPLC, Figure S2) and examined using an Fourier transform infrared (FTIR) spectrometer at Swinburne University of Technology. We discuss this verification further in the Supporting Information but for now point out that the agreement for *Z* is comparable to that for the *E*-RSVL isomer and that the spectra we recorded for *E* are in agreement with those published previously (and reproduced in Figure S1).

3. RESULTS AND DISCUSSION

3.1. Hirshfeld Charges and Molecular Electrostatic Potentials (MEPs). It is known that neither *Z*- nor *E*-RSVL diastereomer has a strictly planar ground-state minimum energy geometry.^{21,49,50} The *E* (trans) form has a very slight twist, with $\sim 6\text{--}7^\circ$ dihedral torsion in each of the single bonds connecting the rings to the stilbene bridge, whereas the bridge itself is locally planar.^{21,49,50} For the *Z* (cis) diastereomer, the nonplanarity is significantly more pronounced because of steric crowding between the phenyl rings in the *Z* configuration. For either diastereomer, nonplanarity manifests via the appearance of paired minima with different helicities, denoted *P* and *M* (see Figure 1). The *P* and *M* conformations of *Z*-RSVL are related by mirror symmetry. In either *Z* or *E* diastereomer, the helical twist of the stilbene bridge is dominated by the twisting of the phenyl rings about their single bonds (refer to ref 25). In the *Z* diastereomer, each of these bonds contributes $\sim 39^\circ$ of twist to

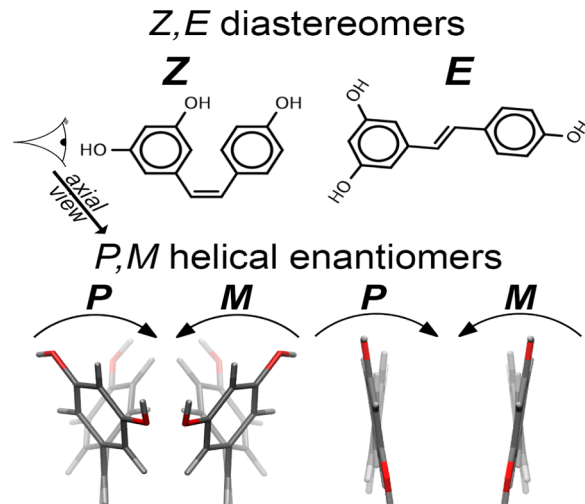


Figure 1. Stereochemical nomenclature for different conformers of resveratrol studied in this article. Each of the *Z* and *E* diastereomeric forms (top) has two ground-state minima, which occur in enantiomeric pairs. Different enantiomeric minima (bottom) are labeled *P* (plus) or *M* (minus) according to their helicity with respect to a right-hand rule (with thumb pointing along the eye's line of sight, from the ring with a higher Cahn–Ingold–Prelog priority (resorcinol) toward that with a lower priority (phenol)).

the bridge, whereas there is only 6° of dihedral torsion in the stilbene bond.⁴⁹

Because of three hydroxyl groups ($-\text{OH}$) on two phenyl rings, resveratrol exhibits a number of conformers (syn- and conrotatory ring positions), as discussed by McNaughton and co-workers.⁴⁹ Using the DFT-based B3LYP/6-31G* model with a smaller basis set, six conformers of *E*-resveratrol with close energies were located.³⁹ The global minimum structure was determined with all of the $-\text{OH}$ groups anticlockwise (the d-structure in ref 49), which is $0.53 \text{ kJ}\cdot\text{mol}^{-1}$ lower in energy than the c-structure in ref 49. The relative energy may also depend on the model and basis set employed. Our study using a model and a larger basis set, that is, B3LYP/6-311++G**, determined that the c-structure in ref 49 (i.e., the $-\text{OH}$ of the phenol ring turns clockwise) is slightly lower in energy than the d-structure for *E*-resveratrol, in agreement with the recent study of Güder et al.⁵⁰ In addition, the calculated NMR chemical shift based on this c-structure also agrees well with NMR measurements.^{21,50}

For either diastereomer, there are two possible routes to exchange the *P* and *M* conformations. The first is to move "through the mirror", overcoming a barrier with at least approximately 2-fold symmetry. Another involves twisting one of the rings the other way by 180° and simultaneously reorienting the OH groups on the chosen ring so as to bring one conformer into its image (Figure 1). A lower bound on the barrier for $P \leftrightarrow M$ exchange can be taken from the previous work, which suggests a barrier of $2.5 \text{ kcal}\cdot\text{mol}^{-1}$ for twisting one of the single bonds.²¹ We obtained an upper bound by optimizing a planar geometry with sufficient strain to allow passage of the hindering sites on the rings and found that this structure was $\sim 7.0 \text{ kcal}\cdot\text{mol}^{-1}$ higher than the *P* and *M* helical minima. A frequency analysis of this structure indicated two imaginary frequencies associated with the syn- and conrotatory ring motions. The magnitude of the synrotatory mode was smaller.^{21,51} The presence of two imaginary modes reflects dual distinguishable sources of stress in the planar structure, both

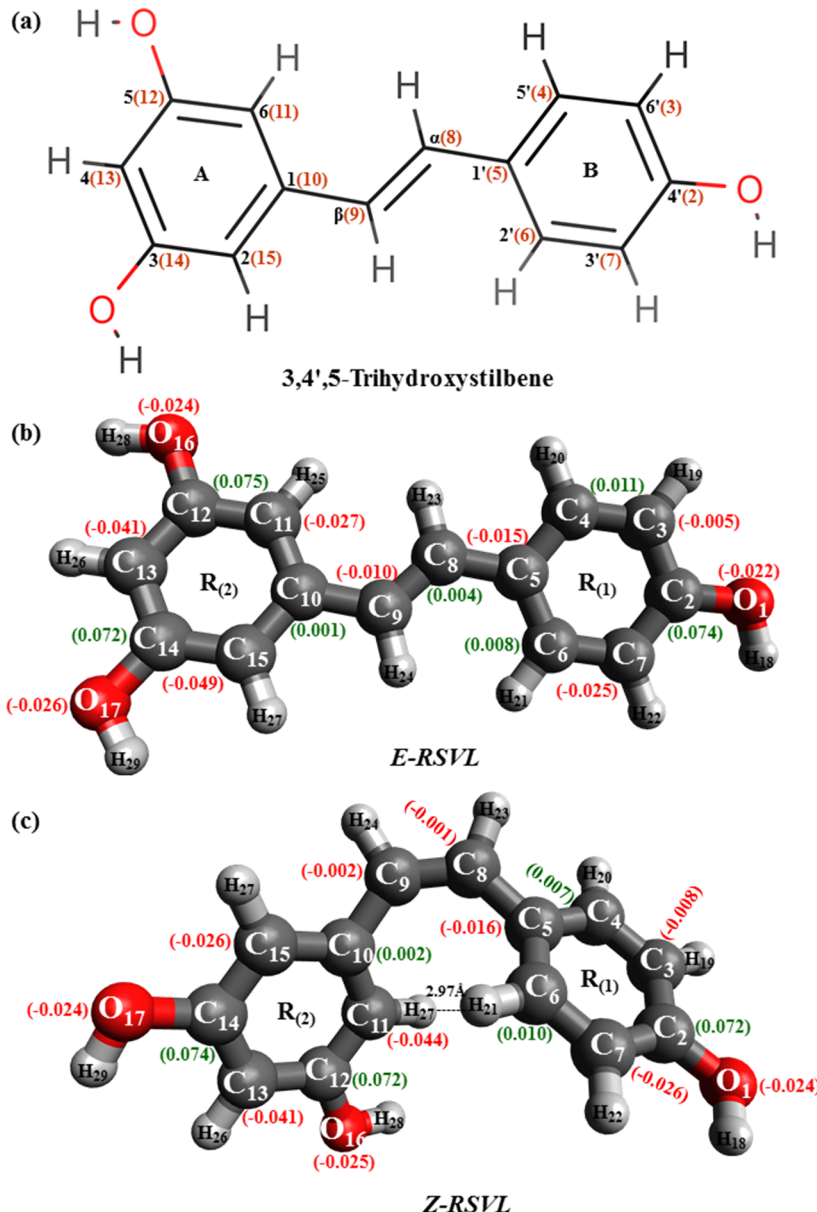


Figure 2. Nomenclature and optimized (three-dimensional, 3D) structures of (b) *E*- and (c) *Z*-RSVL in their ground electronic states using B3LYP/6-311++G**. Hirshfeld charges are present in parentheses, and H-bond distances are also indicated (for IUPAC nomenclature, refer (a)).

the interactions between the rings and those imposed on the rings by the bridge valence structure. The energy estimate of ~ 7.0 kcal·mol $^{-1}$ can be taken as an upper bound to the activation energy for $P \leftrightarrow M$ exchange. Assuming an attempt frequency corresponding to a 100 cm^{-1} vibration (reasonable for ring torsions) at the time scale for $P \leftrightarrow M$ exchange, the rate would lie between 500 ps and 500 ns.

The atom-numbering scheme we used for resveratrol throughout this article is shown in Figure 2. The atomic Hirshfeld charge scheme^{52,53} is employed, and the Hirshfeld charges (Q^H) for the nonhydrogen atoms are also shown for both *E* and *Z* diastereomers in the same figure. The atomic charges are useful in understanding the effect of vibrations on the molecular transition dipole moment, which determines the intensities of spectral lines in the infrared vibrational spectrum. Because of the symmetry, the charges on all atoms in either of the diastereomers are $Q^H < 0.10e$ in magnitude. All charges on the oxygen atoms, $O_{(1)}$, $O_{(16)}$, and $O_{(17)}$, of both *E* and *Z*

diastereomers are largely negative so that the carbon atoms directly bonding with these oxygen atoms, that is, $C_{(2)}$, $C_{(12)}$, and $C_{(14)}$, are positively charged. This pattern is consistent with the electron-donating nature of the para-OH substituent on the phenol ring. A complementary pattern is found for the partial charges on the resorcinol ring, which likewise is consistent with the meta-OH substituents on that ring. As a result, the carbons connecting the stilbene $C=C$ bond and the phenol and resorcinol rings, $C_{(5)}$ and $C_{(10)}$, exhibit alternative charges, one is electron-donating ($C_{(5)}$) and the other is electron-accepting ($C_{(10)}$). There is a notable imbalance of excess negative charges on the two resorcinol sites ortho to the stilbene bridge; the excess negative charge on site $C_{(15)}$ ($Q^H = -0.049e$) is nearly double that of $C_{(11)}$ ($Q^H = -0.027e$) for the *E* diastereomer, whereas for *Z*-RSVL, the order of the charges are swapped, i.e., $C_{(15)}$ ($Q^H = -0.026e$) and $C_{(11)}$ ($Q^H = -0.044e$). Such sensitivity in the charge distribution on the rings to the

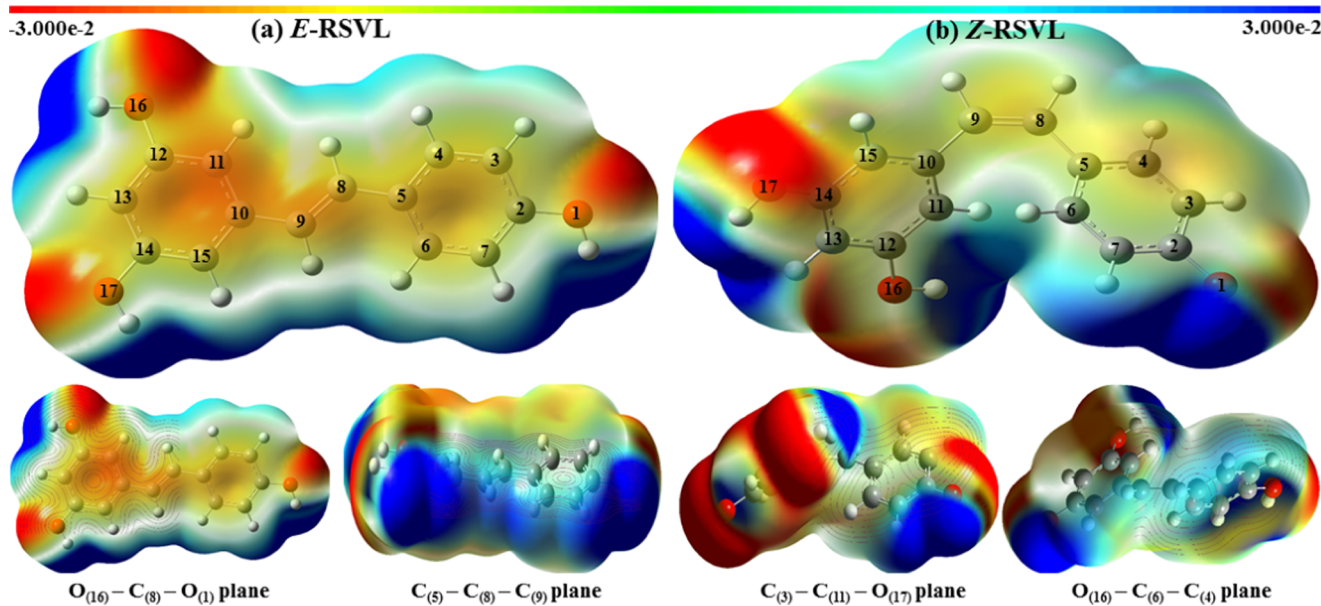


Figure 3. Molecular electrostatic potentials (MEPs) of (a) *E*- and (b) *Z*-RSVL (upper panel) along with their cross sections through the defined planes of MEP maps (lower panel). MEP was calculated using a B3LYP/6-311++G** density functional theory model in vacuum. MEPs are color-coded according to the scale shown at an electronic density isosurface with isovalue 0.004. Red represents negative charges, and blue represents positive charges.

orientation of local dipoles may be relevant to the interaction of resveratrol with other biomolecules.

A number of noticeable differences between the Q^H distributions of *E* and *Z* diastereomers are observed. First, the entire resveratrol carbon frame exhibits alternative positive and negative charges for either *E* or *Z* diastereomers, except for the stilbene bridge, $C_{(8)}=C_{(9)}$, of *Z*-RSVL. Although small, the Q^H values on $C_{(8)}$ and $C_{(9)}$ of *Z*-RSVL have the same negative sign (more electron-donating), that is, $C_{(8)}$ switches from 0.004e in *E*-RSVL to -0.001e in *Z*-RSVL. Next, the majority (two-thirds) of the nonhydrogen atoms exhibits excess negative charges in *Z*-RSVL with respect to those in *E*-RSVL. Only a small number of atomic sites display the opposite charge, that is, the Q^H values on $C_{(6)}$, $C_{(10)}$, and $C_{(14)}$ sites of *Z*-RSVL are more positive than those of *E*-RSVL. Third, as discovered previously,²¹ the most significant changes in Q^H values are observed on sites $C_{(11)}$ and $C_{(15)}$ as they switch their values of Q^H in *E*-RSVL and in *Z*-RSVL. For example, the Q^H values on $C_{(11)}$ and $C_{(15)}$ of *E*-RSVL are -0.027e and -0.049e, respectively, whereas Q^H values on the same carbon sites are -0.044e and -0.026e for *Z*-RSVL. Likely, this is related to the reversal of the local dipolar field accompanying the reorientation of the -OH groups. Finally, the possible intramolecular steric interaction between $H_{(27)}\cdots H_{(21)}$ in *Z*-RSVL (2.97 Å) may contribute to its increase in energy, as represented in Figure 2. The charge redistribution of *Z*-RSVL occurs when the structure becomes more nonplanar.²¹ As revealed in our earlier study,²¹ the $C_{(10)}-C_{(9)}$ bond, which connects the resorcinol ring with the stilbene double $C=C$ bond, is more flexible than the $C_{(8)}-C_{(5)}$ bond connecting the other ring.²¹

An important determinant in the binding of ligands to molecular targets is the molecular electrostatic potential (MEP), which is important for biomolecules. Figure 3 displays the MEPs through some representative molecular planes for both *E* and *Z* diastereomers. The electrostatic potential also indicates the charge distributions of the diastereomers; thus, it

can be an indicator for ligand binding sites with concentrated charges. It also provides the approximate shape of the diastereomers, indicating the matching information when docking to protein pockets. The MEP shown reflects the dominant role of -OH groups in the determination of the molecular charge distribution, with negative potential (red) concentrated in the vicinity of the oxygen atoms and positive potential (blue) localized close to the alcohol hydrogens. More generally, the MEP reflects the character of the C-H bond, with slightly positive potential on the periphery of the molecule, becoming slightly negative nearer to the carbon frame. The highly condensed electron density areas are localized over the oxygen atoms with electron lone pairs. For example, the regions around $O_{(1)}$, $O_{(16)}$, and $O_{(17)}$ in diastereomers show a higher concentration of electrons. Perhaps, the most significant change between *E* and *Z* is when either of the phenol or the resorcinol rings folds over, which brings $H_{(27)}$ and $H_{(21)}$ very close to each other. The MEPs of the *E*- and *Z*-resveratrol have quite different shapes in the 3D space, as shown in the same figure. As a result, the molecular binding activities of the diastereomers are expected to be quite different.

3.2. Vibrational (Simulated Raman and IR) Spectra of *E*- and *Z*-Resveratrol. Simulated Raman scattering spectra of *E* (*trans*) and *Z* (*cis*) RSVL are shown in Figure 4. The Raman spectrum of resveratrol in the present study is dominated by a pair of high-intensity bands in the region of 1609 and 1653 cm^{-1} for *E*-RSVL and 1614 and 1644 cm^{-1} for *Z*-RSVL. The present DFT model produces a slightly more accurate highly intense bands using a scale factor of 0.98 than those from the previous B3LYP/6-31G* model with the smaller basis set and a scale factor of 0.97.⁴⁹ The latter produced the band positions 1615 and 1656 cm^{-1} for *E*-RSVL.⁴⁹ The measured solid-state Raman spectrum exhibits relatively intense band positions at 1589, 1604, 1627, and 1633 cm^{-1} at 532 nm excitation, which is in close alignment with that of resveratrol in 5 mM ethanol solution (after subtraction of the ethanol signals) in the same

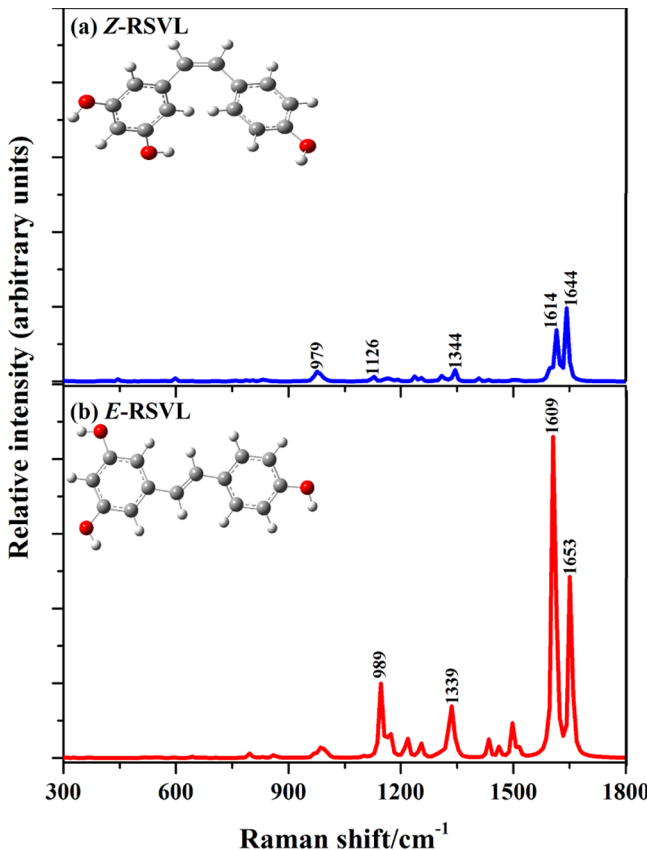


Figure 4. Simulated dual circular polarization (DCP_1) (180°) Raman scattering spectra of *Z* (top) and *E* (bottom) resveratrol. Intensity units are arbitrary, but the spectra are drawn on the same scale. Spectra were simulated using a B3LYP/6-311++G** density functional theory model in vacuum for incident photon energies corresponding to a 532 nm wavelength. Mode frequencies were scaled by a factor of 0.98, and the resulting line spectra were convolved using a Lorentzian distribution with 4 cm^{-1} FWHM. Selected band maxima are shown, as useful to clarify the discussion in the text.

study.⁴⁹ The vibration modes of RSVL above 1500 cm^{-1} are dominated by the double $\text{C}=\text{C}$ bonds, that is, the stilbene $\text{C}=\text{C}$ bond, and other $\text{C}=\text{C}$ bonds in the phenol rings are assigned to the bands at 1609 and 1653 cm^{-1} , in agreement with ref 49. For example, the modes contributing to the smaller wavenumber band (1609 and 1614 cm^{-1}) are assigned to the double $\text{C}_{(13)}=\text{C}_{(14)}$ and $\text{C}_{(6)}=\text{C}_{(7)}$ bond stretches, whereas those contributing to the higher wavenumber band (1644 and 1653 cm^{-1}) are assigned to the stilbene (olefin) $\text{C}_{(8)}=\text{C}_{(9)}$ and ring double-bond stretches. In addition, the two most intense bands at 1609 and 1653 cm^{-1} of *E*-RSVL shift 5 and -9 cm^{-1} inward, respectively, for the nonplanar *Z*-RSVL isomer, leading to the reduction of the spectral gap between two bands from ca. 44 cm^{-1} in *E*-RSVL to ca. 30 cm^{-1} in *Z*-RSVL.

Raman intensities reflect the change in polarizability associated with the displacement along the modes and in the case of resveratrol. Figure 4 reports the calculated Raman spectra of *E*- and *Z*-RSVL up to 1800 cm^{-1} . The Raman spectral intensities of *E*-RSVL are significantly more intense than those of its *Z* counterpart, as shown in Figure 4. In particular, the spectral bands above 1500 cm^{-1} are nearly 10 times more intense in *E*-RSVL than the bands of *Z*-RSVL. In a two-state model, lowering the energy of this structure would increase the polarizability of resveratrol because of the

significant dipole moment associated with the high-energy state. This same picture can also explain the comparatively lower Raman scattering observed in the *cis* (*Z*) form because the closer proximity of the rings implies a smaller dipole moment²¹ and hence a lower contribution to the polarizability. The generally diminished Raman scattering intensity of the *Z* form may be because of the loss of planar symmetry so that the (plane) polarization effect is enhanced on the planar *E*-RSVL rather than on the nonplanar *Z*-RSVL. For example, the very intense Raman spectral band for the *E* form at 1609 cm^{-1} in Figure 2 is nearly 10 times more intense than the same band at 1614 cm^{-1} for the *Z* form. This band is due to $\text{C}=\text{C}$ double bonds, $\text{C}(3)=\text{C}(4)$ and $\text{C}(6)=\text{C}(7)$, stretching in the phenol ring. In addition, the band at 1653 cm^{-1} of the *E* form is also very intense compared with the 1644 cm^{-1} band of the *Z* form in Figure 2, although both of them are assigned to the stilbene bond $\text{C}(8)=\text{C}(9)$ stretching.

Simulated IR spectra for *Z*- and *E*-resveratrol in vacuum are shown in Figure 5 to further explore the properties of *Z*-

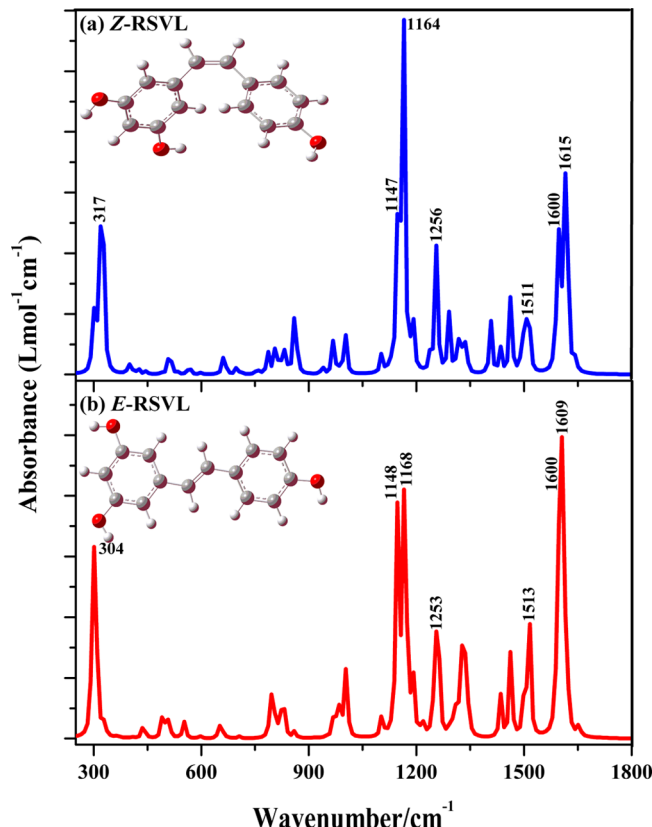


Figure 5. Simulated IR absorbance spectra of *Z* (top) and *E* (bottom) resveratrol in vacuum. Spectra were simulated using a B3LYP/6-311++G** density functional theory model in vacuum for incident photon energies corresponding to a 532 nm wavelength. Mode frequencies were scaled by a factor of 0.98, and the resulting line spectra were convolved using a Lorentzian distribution with 4 cm^{-1} FWHM. Selected band peak positions are indicated in the figure.

resveratrol with respect to *E*-resveratrol. The IR spectral shift is noted, and the IR assignments of the diastereomers are given in Table S1. An excellent agreement between the experimentally measured and theoretically calculated spectra was achieved with a mean signed error being $<1.00\text{ cm}^{-1}$ in acetonitrile ($\epsilon = 37.5$) solution. For example, the bendings of $\text{C}-\text{H}$ ring $\text{R}_{(1)}$, that is, phenol ring, and ring wag $\text{R}_{(2)}$, that is, resorcinol ring, of *E*-

RSVL are 1515 and 661 cm^{-1} , respectively, which are in close agreement with those measured at 1514 and 661 cm^{-1} . The excellent agreement between the calculated and measured frequencies for *E* (*trans*) and *Z* (*cis*) RSVL indicates that the B3LYP/6-311++G** model is reliable to produce accurate IR results for these diastereomers. This finding is in agreement with recent DFT functional performance assessment studies^{54,55} that the overall performance of the B3LYP method on a number of isotropic properties is consistently high.

Unlike the Raman spectrum, which exhibits a cluster of high bands in the region of 1600–1653 cm^{-1} in *E*-RSVL, the IR spectra for both diastereomers of RSVL show bands with competitive intensity in the same IR fingerprint region of ca. 300–1750 cm^{-1} with two clusters of intense bands in high, 1600–1615 cm^{-1} , and low, 1147–1168 cm^{-1} , regions. The intensity appears to redistribute between the bands in the high (1600–1615 cm^{-1}) and low (1147–1168 cm^{-1}) wavenumber features for the *Z* and *E* diastereomers. These bands are combinations of bond stretches and hybridization angle wags on the substituted rings. As shown in the atomic Hirshfeld charge analysis (Figure 2), the excess charge density on the ring atoms has alternative signs; the nearest neighbors have opposite excess charge densities. As a result, local bond vibrations on the rings are coupled to the permanent charge moments, giving significant transition dipole moment changes and therefore the IR intensity. Figure 5 obviously indicates that the spectra are different but the structures are related.

The Raman and IR spectra indeed exhibit interesting features unique to the individual resveratrol diastereomers. The energy difference between the *E* and *Z* diastereomers is calculated to be 4.30 $\text{kcal}\cdot\text{mol}^{-1}$ using the same DFT model that was used in our previous study,²¹ whereas the ground-state energy barrier for thermal *E* \leftrightarrow *Z* isomerization is significant at 43.6 $\text{kcal}\cdot\text{mol}^{-1}$.⁵⁷ The excited state barrier is much smaller, and irradiation of the *E* diastereomer produces a mixture of *E* and *Z*.²⁴ Figures 4 and 5 indicate that both *E*- and *Z*-RSVL are IR-active as the transition dipole moment is not affected significantly by the positions of the phenol rings on the opposite sides (*E*-RSVL) or on the same side (*Z*-RSVL) of the stilbene $\text{C}_{(8)}=\text{C}_{(9)}$ bond. However, the positions of the phenol rings may significantly discriminate the polarizability and therefore the Raman spectrum of *Z*-RSVL when on the same side of the stilbene $\text{C}=\text{C}$ bond.

3.3. Vibrational Optical Activity Spectra. It has been shown that RSVL presents torsional flexibility around the two C–C bonds connecting the stilbene $\text{C}_{(8)}=\text{C}_{(9)}$ to the phenyl groups.²¹ Circular dichroism (CD) and Raman optical activity (ROA) may provide information about the structure and symmetry of the isomers because the sign, shape, and intensity of the vibrational circular dichroism (VCD) and ROA spectra are structure- and symmetry-dependent. This study examines optical activity signatures that may arise if an enantiomeric excess of one helical conformer were to arise, for example, by interaction with an external chiral influence. Figure 6 presents the simulated ROA, and Figure 7 reports the IR VCD, both calculated using the same DFT model for the *P*–*E* and *M*–*Z*-RSVL diastereomers. As seen in the spectra, the optical signals reported in the ROA and VCD spectra of the *E*- and *Z*-resveratrol diastereomers are significantly different, indicating their significant chirality. The corresponding spectra for the *M*–*E* and *P*–*Z* conformers could be generated as the negative of the spectra in Figures 6 and 7. In the absence of an external

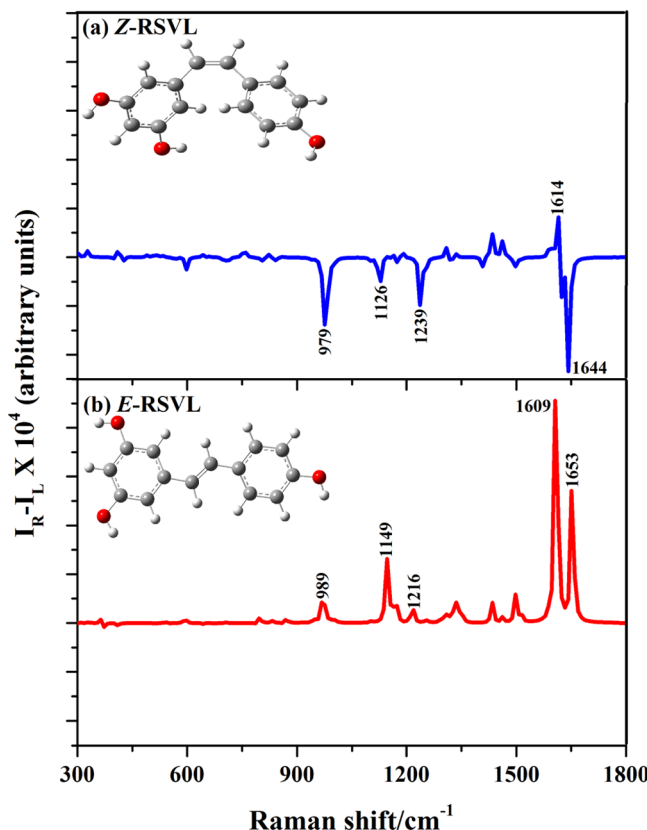


Figure 6. Simulated ROA spectra of *E*- and *Z*-resveratrol using the B3LYP/6-311++G** model at 532 nm excitation wavelength in vacuum. Absorbance units are arbitrary, but spectra are plotted on comparable scales. Mode frequencies were scaled by a factor of 0.98.

chiral influence, the spectra will cancel and no optical activity would be expected.

Although the *E*-RSVL diastereomer displays significantly stronger signals (ca. 10 times) in its Raman spectrum (Figure 4) with respect to those of *Z*-RSVL, its ROA signals are less intense. The ROA spectra of the *E* conformers are nearly monosignate; all signals with sufficiently large ROA intensities of *P*–*E*-RSVL are positive. Such a spectrum may be expected in the presence of an external chiral influence generating an excess of the *P*-helical enantiomer, as shown in Figure 1 (and Figure S2). On the other hand, the ROA signals of *M*–*Z*-RSVL are sufficiently intense with signals on both positive and negative sides. This suggests that in the presence of an external chiral influence a bisignate ROA spectrum is likely to be observed for the *Z* diastereomer.

Figure 7 reports the simulated VCD for both *P*–*E* and *M*–*Z*-RSVL. Although the IR spectra of *E*- and *Z*-RSVL isomers exhibit competitively strong signals (see Figure 5), the VCD spectra of *P*–*E*-RSVL show merely small and negligible residual signals. However, the VCD signals on both sides of the *M*–*Z*-RSVL spectrum are more intense. The VCD spectral bands at 1600 and 1164 cm^{-1} show apparent residual signals. For example, the higher-energy band (1600 cm^{-1}) is due to an intense mode composed of $\text{C}=\text{C}$ in the stilbene and ring vibrations on the resorcinol and the phenol rings, whereas the lower-energy band (1165 cm^{-1}) is dominated by out-of-plane motion of the $\text{C}_{(6)}$ carbon atom in the phenol ring. Similarly, the ROA spectra of *M*–*Z*-resveratrol in Figure 6 show that there is a significant optical rotation strength in the bands at

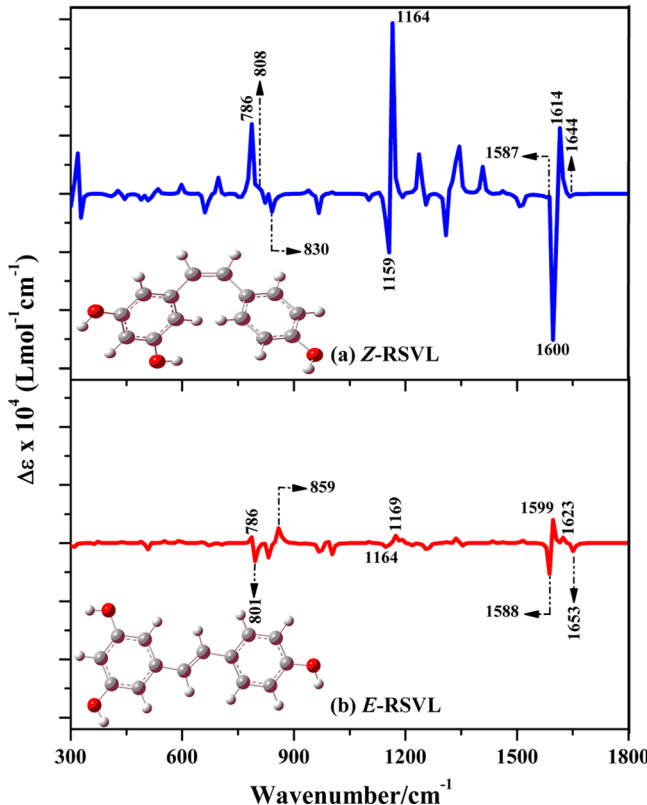


Figure 7. Simulated VCD spectra of *P*–*E* and *M*–*Z*-resveratrol using the B3LYP/6-311++G** model in vacuum. Absorbance units are arbitrary, but spectra are plotted on comparable scales. Mode frequencies were scaled by a factor of 0.98.

1614–1644 cm^{-1} , which also dominate the Raman scattering spectrum. Interestingly, the ROA spectra in Figure 6 and VCD spectra in Figure 7 show apparent differences for the *E* and *Z* forms, indicating different configurations and chiralities of the *Z* and *E* forms of RSVL. The magnitudes of the VCD spectrum of the *Z* form (Figure 7) are significantly more intense than the very weak VCD signals of the *E* form, whereas the signals in the ROA spectrum of the *Z* form show both positive and negative signals, but the negative signals in the same spectrum of the *E* form are negligibly small.

The binding of *P*–*Z*-resveratrol to human tyrosyl-tRNA synthetase has recently been demonstrated by a solution of the co-crystal structure of the complex.³⁰ At the time of writing, this was the only structure in the protein data bank (PDB) that included *Z*-resveratrol as a ligand and only the *P* conformer was observed. The binding inhibits the synthetase and directs it to a nuclear function where it is implicated in the initiation of the stress response. The tyrosyl-tRNA synthetase binds *P*–*Z*-resveratrol better than it does tyrosine. Structural differences relative to the tyrosine-bound synthetase show that the binding is coupled to a conformational change, which opens a pocket to accommodate the resorcinol ring.³⁰ It has been suggested³⁰ that this conformational change may be driving the conversion of the *E* diastereomer, which is prevalent in solution, to the bound *Z* diastereomer.

A primary motivation for this work is the information that the optical activities of resveratrol might be used to optically detect the binding of resveratrol to the human-tRNA synthetase. Because the co-crystal structure was observed to bind only the *P* atropisomer, the accumulation of bound *Z*

resveratrol should lead to an enantiomeric excess of *P*. This explains the reasons for our examination of the VCD and ROA spectra shown in Figure S3. Optical activity is not expected for *Z*-resveratrol in room-temperature solution, as the helical atropisomers are isoenergetic and exchange on the picosecond–nanosecond time scale.

Interaction with protein may stabilize the *P* conformer over *M* or raise the barrier to $P \leftrightarrow M$ exchange. Scheme 2 shows the schematic representation of *Z*-resveratrol in the binding pocket, indicating a hydrogen bond between residue E170 and one of the resorcinol alcohol groups.³⁰ It is unlikely that this bond would form in the *M* conformer, as the relevant alcohol group may not be in a position to form the bond. Hydrogen bond energies in chemistry and biology span a fairly broad range of typically 0.2–40 kcal·mol⁻¹¹⁵⁶ and thus the energy could be sufficient to stabilize the *P* conformer over *M*. The barrier to $P \leftrightarrow M$ exchange in bound *Z*-resveratrol could be calculated explicitly in a detailed model, which is beyond the scope of this study.

The VCD and ROA spectra of *P*–*Z*-resveratrol (Figure S3) are each dominated by a different intense pair of lines. The ROA spectrum is dominated by a monosignate pair of lines at 1644 and 979 cm^{-1} . The VCD spectrum is dominated by a bisignate pair of lines at 1600 and 1165 cm^{-1} . We propose that these lines may be used to detect the binding of *Z*-resveratrol (in the *P* conformation) to the tyrosyl-tRNA synthetase. *Z*-resveratrol in solution will exist as a racemic mixture, without observable optical activity. The accumulation of the bound form should appear as a change in the optical activity relative to that of a solution of unbound synthetase. The ROA line at 1644 cm^{-1} lies very close to the protein amide I band, which may complicate the detection, but the line at 979 cm^{-1} does not lie in the immediate vicinity of any of the amide bands. This is useful because the amide bands are sensitive to the structure and thus binding of resveratrol could change the spectrum by altering the structure as well as by its own optical activity. Likewise, in the VCD spectra, the proximity of the band at 1600 cm^{-1} to the amide I and II bands could also complicate the detection, but the 1165 cm^{-1} band is well removed from these bands.

The units of the spectra in Figures 4–7 are arbitrary, but a comparison against similar molecules for which computational results and experimental spectra are available suggests that the signal is in a range that should be detectable with modern techniques and instrumentation.^{58,59}

4. CONCLUSIONS

We have reported vibrational spectra of the *E* and *Z* diastereomers of resveratrol, with the intention of identifying if and which features may be used to detect the presence of *Z*-resveratrol bound to the human tyrosyl-tRNA synthetase.³⁰ We have shown that *Z*-resveratrol exists as two nonplanar helical atropisomers (*P*–*Z*-RSVL and *M*–*Z*-RSVL) with opposite vibrational optical activity spectra. These forms exchange in solution on a fast time scale, so that unbound *Z*-resveratrol should be racemic and invisible in these spectra. However, because the synthetase is observed to bind only one of them (*P*–*Z*-RSVL), the accumulation of bound *Z*-resveratrol is expected to create an enantiomeric excess, which can be detected via the optical activity spectra and vibrational circular dichroism spectra. We have identified chirality of *Z*-RSVL in the spectra that are most likely to be useful for the detection of bound *Z*-resveratrol.

■ ASSOCIATED CONTENT

§ Supporting Information

The Supporting Information is available free of charge on the ACS Publications website at DOI: [10.1021/acs.jpcb.7b10278](https://doi.org/10.1021/acs.jpcb.7b10278).

Experimental method for HPLC and FTIR; experimental and simulated Raman and infrared spectra comparison for *E*-RSVL (Figure S1); HPLC chromatography of *E*-RSVL, before and after the exposure to UV radiation along with its comparison with a wine sample (Figure S2); simulated Raman/ROA and IR/VCD of *Z*-RSVL, capturing the helical atropomers *P* and *M* (Figure S3); measured and calculated vibrational fundamentals of resveratrol (Table S1); results and discussion for vibrational and VOA spectra for Figure S3 and Table S1 ([PDF](#))

■ AUTHOR INFORMATION

Corresponding Author

*E-mail: fwang@swin.edu.au. Tel: +61 3 9214 5056. Fax: +61 3-9214-5921.

ORCID

Seth Olsen: [0000-0002-3822-753X](https://orcid.org/0000-0002-3822-753X)
Feng Wang: [0000-0002-6584-0516](https://orcid.org/0000-0002-6584-0516)

Author Contributions

The manuscript was written through contributions of all authors. All authors have given approval to the final version of the manuscript.

Notes

The authors declare no competing financial interest.

■ ACKNOWLEDGMENTS

F.W. acknowledges the Australia Research Council (ARC) through the Discovery Project (DP) for funding and PhD scholarship for S.C. S.C. acknowledges Prof. Ferenc Billes from Department of Physical Chemistry, Budapest University of Technology and Economics, Hungary, for sharing the experimental Raman data for *E*-resveratrol. The authors also acknowledge the merit-based supercomputing time from National Computational Infrastructure (NCI) and Swinburne University Supercomputing Facility. Finally, F.W. acknowledges the Swinburne University of Technology for financial support of her Academic Sabbatical Award hosted by the School of Chemistry (Bio21 Institute) and School of Physics, University of Melbourne.

■ DEDICATION

#This article is in memory of our colleague and friend Dr. Seth Olsen who passed away in 2018.

■ REFERENCES

- (1) Keylor, M. H.; Matsuura, B. S.; Stephenson, C. R. J. Chemistry and biology of resveratrol-derived natural products. *Chem. Rev.* **2015**, *115*, 8976–9027.
- (2) Burns, J.; Yokota, T.; Ashihara, H.; Lean, M. E. J.; Crozier, A. Plant foods and herbal sources of resveratrol. *J. Agric. Food Chem.* **2002**, *50*, 3337–3340.
- (3) Frankel, E. N.; Kanner, J.; German, J. B.; Parks, E.; Kinsella, J. E. Inhibition of oxidation of human low-density lipoprotein by phenolic substances in red wine. *Lancet* **1993**, *341*, 454–457.
- (4) Biagi, M.; Bertelli, A. A. Wine, alcohol and pills: What future for french paradox? *Life Sci.* **2015**, *131*, 19–22.
- (5) Quideau, S.; Deffieux, D.; Pouysegur, L. Resveratrol still has something to say about aging! *Angew. Chem., Int. Ed.* **2012**, *51*, 6824–6826.
- (6) Baur, J. A.; Sinclair, D. A. Therapeutic potential of resveratrol: The in vivo evidence. *Nat. Rev. Drug Discovery* **2006**, *5*, 493–506.
- (7) Tennen, R. I.; Michishita-Kioi, E.; Chua, K. F. Finding a target for resveratrol. *Cell* **2012**, *148*, 387–389.
- (8) Park, S. J.; Ahmad, F.; Philp, A.; Baar, K.; Williams, T.; Luo, H.; Ke, H.; Rehmann, H.; Taussig, R.; Brown, A. L.; et al. Resveratrol ameliorates aging-related metabolic phenotypes by inhibiting cAMP phosphodiesterases. *Cell* **2012**, *148*, 421–433.
- (9) Vang, O.; Ahmad, N.; Baile, C. A.; Baur, J. A.; Brown, K.; Csiszar, A.; Das, D. K.; Delmas, D.; Gottfried, C.; Lin, H. Y.; et al. What is new for an old molecule? Systematic review and recommendations on the use of resveratrol. *PLoS One* **2011**, *6*, No. e19881.
- (10) Baur, J. A.; Pearson, K. J.; Price, N. L.; Jamieson, H. A.; Lerin, C.; Kalra, A.; Prabhu, V. V.; Allard, J. S.; Lopez-Lluch, G.; Lewis, K.; et al. Resveratrol improves health and survival of mice on a high-calorie diet. *Nature* **2006**, *444*, 337–342.
- (11) Wood, J. G.; Rogina, B.; Lavu, S.; Howitz, K.; Helfand, S. L.; Tatar, M.; Sinclair, D. Sirtuin activators mimic caloric restriction and delay ageing in metazoans. *Nature* **2004**, *430*, 686–689.
- (12) Leiro, J.; Alvarez, E.; Arranz, J. A.; Laguna, R.; Uriarte, E.; Orallo, F. Effects of *cis*-resveratrol on inflammatory murine macrophages: Antioxidant activity and down-regulation of inflammatory genes. *J. Leukocyte Biol.* **2004**, *75*, 1156–1165.
- (13) Bradamante, S.; Barenghi, L.; Villa, A. Cardiovascular protective effects of resveratrol. *Cardiovasc. Drug Rev.* **2004**, *22*, 169–188.
- (14) Aggarwal, B. B.; Bhardwaj, A.; Aggarwal, R. S.; Seeram, N. P.; Shishodia, S.; Takada, Y. Role of resveratrol in prevention and therapy of cancer: Preclinical and clinical studies. *Anticancer Res.* **2004**, *24*, 2783–2840.
- (15) Leonard, S. S.; Xia, C.; Jiang, B. H.; Stinefelt, B.; Klandorf, H.; Harris, G. K.; Shi, X. Resveratrol scavenges reactive oxygen species and effects radical-induced cellular responses. *Biochem. Biophys. Res. Commun.* **2003**, *309*, 1017–1026.
- (16) Wang, Q.; Xu, J.; Rottinghaus, G. E.; Simonyi, A.; Lubahn, D.; Sun, G. Y.; Sun, A. Y. Resveratrol protects against global cerebral ischemic injury in gerbils. *Brain Res.* **2002**, *958*, 439–447.
- (17) Soleas, G. J.; Diamandis, E. P.; Goldberg, D. M. Resveratrol: a molecule whose time has come? And gone? *Clin. Biochem.* **1997**, *30*, 91–113.
- (18) Gehm, B. D.; McAndrews, J. M.; Chien, P. Y.; Jameson, J. L. Resveratrol, a polyphenolic compound found in grapes and wines, is an agonist for the estrogen receptor. *Proc. Natl. Acad. Sci. U.S.A.* **1997**, *94*, 14138–14143.
- (19) Deak, M.; Falk, H. On the chemistry of the resveratrol diastereomers. *Monatsh. Chem.* **2003**, *134*, 883–888.
- (20) Trella, B. C.; Waterhouse, A. L. Resveratrol: Isomeric molar absorptivities and stability. *J. Agric. Food Chem.* **1996**, *44*, 1253–1257.
- (21) Wang, F.; Chatterjee, S. Dominant carbons in trans and cis-resveratrol isomerization. *J. Phys. Chem. B* **2017**, *121*, 4745–4755.
- (22) Jeandet, P.; Bessis, R.; Maume, B. F.; Meunier, P.; Peyron, D.; Trollat, P. Effect of enological practices on the resveratrol isomer content of wine. *J. Agric. Food Chem.* **1995**, *43*, 316–319.
- (23) Simkovich, R.; Huppert, D. Excited-state proton transfer in resveratrol and proposed mechanism for plant resistance to fungal infection. *J. Phys. Chem. B* **2015**, *119*, 11684–11694.
- (24) Figueiras, T. S.; Neves-Petersen, M. T.; Petersen, S. B. Activation energy of light induced isomerization of resveratrol. *J. Fluoresc.* **2011**, *21*, 1897–1906.
- (25) Abou-Zeid, L. A.; El-Mowafy, A. M. Differential recognition of resveratrol isomers by the human estrogen receptor- α : Molecular dynamics evidence for stereoselective ligand binding. *Chirality* **2004**, *16*, 190–195.
- (26) Howitz, K. T.; Bitterman, K. J.; Cohen, H. Y.; Lamming, D. W.; Lavu, S.; Wood, J. G.; Zipkin, R. E.; Chung, P.; Kisielewski, A.; Zhang, L.; et al. Small molecule activators of sirtuins extended *Saccharomyces cerevisiae* lifespan. *Nature* **2003**, *425*, 191–196.

- (27) Ford, R. J.; Desjardins, E. M.; Steinberg, G. R. Are SIRT1 activators another indirect method to increase AMPK for beneficial effects on aging and the metabolic syndrome? *EBioMedicine* **2017**, *19*, 16–17.
- (28) Price, N. L.; Gomes, A. P.; Ling, A. J. Y.; Duarte, F. V.; Martin-Montalvo, A.; North, B. J.; Agarwal, B.; Ye, L.; Ramadori, G.; Teodoro, J. S.; et al. SIRT1 is required for AMPK activation and the beneficial effects of resveratrol on mitochondrial function. *Cell Metab.* **2012**, *15*, 675–690.
- (29) Viswanathan, M.; Kim, S. K.; Berdichevsky, A.; Guarente, L. A role for SIR-2.1 regulation of ER stress response genes in determining *C. elegans* life span. *Dev. Cell* **2005**, *9*, 605–615.
- (30) Sajish, M.; Schimmel, P. A human tRNA synthetase is a potent PARP1-activating effector target for resveratrol. *Nature* **2015**, *519*, 370–373.
- (31) Fu, G.; Xu, T.; Shi, Y.; Wei, N.; Yang, X. L. tRNA-controlled nuclear import of a human tRNA synthetase. *J. Biol. Chem.* **2012**, *287*, 9330–9334.
- (32) Billes, F.; Mohammed-Ziegler, I.; Mikosch, H.; Tyihak, E. Vibrational spectroscopy of resveratrol. *Spectrochim. Acta, Part A* **2007**, *68*, 669–679.
- (33) Becke, A. D. Density-functional exchange-energy approximation with correct asymptotic behavior. *Phys. Rev. A* **1988**, *38*, 3098–3100.
- (34) Lee, C.; Yang, W.; Parr, R. G. Development of the Colle–Salvetti correlation-energy formula into a functional of the electron density. *Phys. Rev. B* **1988**, *37*, 785–789.
- (35) Krishnan, R.; Binkley, J.; Seeger, R.; Pople, J. A. Self-consistent molecular orbital methods. XX. A basis set for correlated wave functions. *J. Chem. Phys.* **1980**, *72*, 650–654.
- (36) Clark, T.; Chandrasekhar, J.; Spitznagel, G.; Schleyer, P. V. R. Efficient diffuse function-augmented basis sets for anion calculations. III. The 3-21+G basis set for first-row elements, Li–F. *J. Comput. Chem.* **1983**, *4*, 294–301.
- (37) Becke, A. D. Density-functional thermochemistry. III. The role of exact exchange. *J. Chem. Phys.* **1993**, *98*, 5648–5652.
- (38) Zvereva, E. E.; Shagidullin, A. R.; Katsyuba, S. A. Ab initio and DFT predictions of infrared intensities and Raman activities. *J. Phys. Chem. A* **2011**, *115*, 63–69.
- (39) Falzon, C. T.; Wang, F. Understanding glycine conformation through molecular orbitals. *J. Chem. Phys.* **2005**, *123*, No. 214307.
- (40) Falzon, C. T.; Wang, F.; Pang, W. Orbital signatures of methyl in L-alanine. *J. Phys. Chem. B* **2006**, *110*, 9713–9719.
- (41) Ganeshan, A.; Wang, F. Intramolecular interactions of L-phenylalanine revealed by inner shell chemical shift. *J. Chem. Phys.* **2009**, *131*, No. 0444321.
- (42) Ganeshan, A.; Wang, F.; Falzon, C. Intramolecular interactions of L-phenylalanine: Valence ionization spectra and orbital momentum distributions of its fragment molecules. *J. Comput. Chem.* **2011**, *32*, 525–535.
- (43) Ganeshan, A.; Wang, F.; Brunger, M.; Prince, K. Effects of alkyl side chains on properties of aliphatic amino acids probed using quantum chemical calculations. *J. Synchrotron Radiat.* **2011**, *18*, 733–742.
- (44) Frisch, M. J.; Trucks, G. W.; Schlegel, H. B.; Scuseria, G. E.; Robb, M. A.; Cheeseman, J. R.; Scalmani, G.; Barone, V.; Mennucci, B.; Petersson, G. A.; et al. *Gaussian 09*, revision A.1; Gaussian, Inc.: Wallingford, CT, 2009.
- (45) Cheeseman, J. R.; Frisch, M. J.; Devlin, F. J.; Stephens, P. J. *Ab initio* calculation of atomic axial tensors and vibrational rotational strengths using density functional theory. *Chem. Phys. Lett.* **1996**, *252*, 211–220.
- (46) Stephens, P. J. Theory of vibrational circular dichroism. *J. Phys. Chem.* **1985**, *89*, 748–752.
- (47) Cossi, M.; Rega, N.; Scalmani, G.; Barone, V. Energies, structures, and electronic properties of molecules in solution with the C-PCM solvation model. *J. Comput. Chem.* **2003**, *24*, 669–681.
- (48) Gawronski, J. K.; Kwit, M.; Boyd, D. R.; Sharma, N. D.; Malone, J. F.; Drake, A. F. Absolute configuration, conformation, and circular dichroism of monocyclic arene dihydrodiol metabolites: it is all due to the heteroatom substituents. *J. Am. Chem. Soc.* **2005**, *127*, 4308–4319.
- (49) Vongsvivut, J.; Robertson, E. G.; McNaughton, D. Surface-enhanced Raman scattering spectroscopy of resveratrol. *Aust. J. Chem.* **2008**, *61*, 921–929.
- (50) Güder, A.; Korkmaz, H.; Gokce, H.; Alpaslan, Y. B.; Alpaslan, G. Isolation, characterization, spectroscopic properties and quantum chemical computations of an important phytoalexin resveratrol as antioxidant component from *Vitis labrusca* L. and their chemical compositions. *Spectrochim. Acta, Part A* **2014**, *133*, 378–395.
- (51) Pour, S. O.; Rocks, L.; Faulds, K.; Graham, D.; Parchansky, V.; Bour, P.; Blanch, E. W. Through-space transfer of chiral information mediated by a plasmonic nanomaterial. *Nat. Chem.* **2015**, *7*, 591–596.
- (52) Chatterjee, S.; Ahmed, M.; Wang, F. How similar is the electronic structures of β -lactam and alanine? *Radiat. Phys. Chem.* **2016**, *119*, 1–8.
- (53) Hirshfeld, F. L. Bonded-atom fragments for describing molecular charge densities. *Theor. Chem. Acc.* **1977**, *44*, 129–138.
- (54) Wang, F.; Pang, W. N.; Duffy, P. Performance assessment of density functional theory-based models using orbital momentum distributions. *Mol. Simul.* **2012**, *38*, 468–480.
- (55) Zhang, G.; Musgrave, C. B. Comparison of DFT methods for molecular orbital eigenvalue calculations. *J. Phys. Chem. A* **2007**, *111*, 1554–1561.
- (56) Torshin, I. Y.; Weber, I. T.; Harrison, R. W. Geometric criteria of hydrogen bonds in proteins and identification of “bifurcated” hydrogen bonds. *Protein Eng.* **2002**, *15*, 359–363.
- (57) Rodríguez, R. Á.; Lahoz, I. R.; Faza, O. N.; Cid, M. M.; Lopez, C. S. Theoretical and experimental exploration of the photochemistry of resveratrol: beyond the simple double bond isomerization. *Org. Biomol. Chem.* **2012**, *10*, 9175–9182.
- (58) Shingae, T.; Kubota, K.; Kumauchi, M.; Tokunaga, F.; Unno, M. Raman optical activity probing structural deformations of the 4-hydroxycinnamyl chromophore in photoactive yellow protein. *J. Phys. Chem. Lett.* **2013**, *4*, 1322–1327.
- (59) Kubota, K.; Shingae, T.; Foster, N. D.; Kumauchi, M.; Hoff, W. D.; Unno, M. Active site structure of photoactive yellow protein with a locked chromophore analogue revealed by near-infrared raman optical activity. *J. Phys. Chem. Lett.* **2013**, *4*, 3031–3038.